https://doi.org/10.61092/iaea.mrpt-xx9q

INDC(NDS)-0825
Distr. FE,G

IAEA
International Atomic Energy Agency

INDC International Nuclear Data Committee

Processing La-139 in the Unresolved Resonance Region for the FENDL Library

Daniel López Aldama
Center for Technology Applications and Nuclear Development
Havana, Cuba

Roberto Capote Noy
International Atomic Energy Agency (IAEA)
Vienna, Austria

January 2021

IAEA Nuclear Data Section
Vienna International Centre, P.O. Box 100, 1400 Vienna, Austria

Selected INDC documents may be downloaded in electronic form from
http://nds.iaea.org/publications
or sent as an e-mail attachment.
Requests for hardcopy or e-mail transmittal should be directed to
NDS.Contact-Point@iaea.org
or to:
Nuclear Data Section
International Atomic Energy Agency
Vienna International Centre
PO Box 100
1400 Vienna
Austria

Printed by the IAEA in Austria

January 2021

INDC(NDS)-0825
Distr. F,G

Processing La-139 in the Unresolved Resonance Region for the FENDL Library

Daniel López Aldama
Center for Technology Applications and Nuclear Development
Havana, Cuba

Roberto Capote Noy
International Atomic Energy Agency (IAEA)
Vienna, Austria

ABSTRACT

The analysis of a numerical benchmark for a pure 1-meter sphere of La-139 proposed by C. Konno using ACE- and MATXS-formatted cross section files from the FENDL-3.1c library showed problems in the unresolved resonance region (URR). The total neutron flux computed using MCNP/ACE differed up to 50% from the one calculated applying ANISN/MATXS. The problem arose when too small total cross section values were sampled by the PURR module of NJOY2016 mainly due to the limitations of the processing method. NJOY2016 (PURR) patch to correct this issue was proposed and applied. The patch increases the neutron flux in the URR for Monte Carlo calculations (4% increase for the ENDF/B-VIII.0 evaluation vs 30% for the FENDL-3.1c evaluation). The corresponding increase of the calculated neutron flux for deterministic codes goes from 15% for the ENDF/B-VIII.0 data up to 50% for the FENDL-3.1c. The agreement between deterministic and Monte Carlo benchmark results was significantly improved. This report documents the NJOY2016 patch and summarizes the main results.

January 2021

Contents

1. Introduction

The moments of the neutron flux in the resonance energy range according to Bondarenko model [1, 2] for treating self-shielding can be estimated as:

$$\phi_l^i(E) = \frac{C(E)}{\left(\sigma_t^i(E) + \sigma_0^i\right)^{l+1}} \quad (1)$$

where,

$\phi_l^i(E)$: *l-th* moment of the neutron flux for the isotope *i* as a function of energy

C(E): Smooth function of energy, $C(E) \propto \frac{1}{E}$

$\sigma_t^i(E)$: Microscopic total cross section of isotope *i*

σ_0^i: Lumped microscopic cross section. It takes into account all the other isotopes existing in the mixture and the heterogeneity of the system. The values of σ_0^i depend on the resonance model: Narrow Resonance (NR), wide resonance infinite absorber (WRIA) or intermediate resonance (IR) approximation [1, 2]. Usually, σ_0^i is called Bondarenko background cross section.

In the unresolved energy range, it is not possible to define pointwise values for the cross sections of the resonant reactions (total, elastic, fission and capture). It is only possible to define average values conserving the reactions rates. Assuming that expression (1) for the flux moments holds, the average cross section of the reaction x at energy E_m at a given temperature *T* can be calculated for the isotope *i* as:

$$\sigma_x^l(E_m, \sigma_0) = \frac{\int_{E_1}^{E_2} \sigma_x(E)\phi_l(E)dE}{\int_{E_1}^{E_2} \phi_l(E)dE} = \frac{\int_{E_1}^{E_2} \frac{C(E)\sigma_x(E)}{[\sigma_t(E)+\sigma_0]^{l+1}}dE}{\int_{E_1}^{E_2} \frac{C(E)}{[\sigma_t(E)+\sigma_0]^{l+1}}dE} \quad (2)$$

where,

$\sigma_x^l(E_m, \sigma_0)$: The *l-th* moment of the microscopic cross section for reaction x (x=total, elastic, fission and capture) averaged in the energy interval [E_1, E_2].

E_m: Some effective energy in the interval (E_1, E_2). The average value $\sigma_x^l(E_m, \sigma_0)$ is associated to this energy value.

$\sigma_x(E)$: Microscopic cross section for reaction x as a function of energy *E*

The rest of parameters have the same meaning as before, but the isotope index *i* has been dropped to simplify the expressions.

Equation (2) for the zero and the first moment of the cross sections reduces to

$$\sigma_x(E_m,\sigma_0)=\frac{\int_{E_1}^{E_2}\frac{\sigma_x(E)C(E)}{[\sigma_t(E)+\sigma_0]}dE}{\int_{E_1}^{E_2}\frac{C(E)}{[\sigma_t(E)+\sigma_0]}dE}, \qquad \textit{for l=0} \qquad (3)$$

$$\sigma_x^1(E_m,\sigma_0)=\frac{\int_{E_1}^{E_2}\frac{\sigma_x(E)C(E)}{[\sigma_t(E)+\sigma_0]^2}dE}{\int_{E_1}^{E_2}\frac{C(E)}{[\sigma_t(E)+\sigma_0]^2}dE}, \qquad \textit{for l=1} \qquad (4)$$

Equations (3) and (4) represent the zero and first order Bondarenko cross sections. It is worthy to note, that they are average cross-section values associated to E_m, not pointwise data.

In general, the Bondarenko cross sections depend on the lumped cross section σ_0 and the temperature *T*. The most common approach is to prepare a cross section library using an appropriate set of σ_0 values at several temperatures. It is strongly recommended to choose a customized grid of σ_0 and *T* according to the compositions, geometries, dimensions and temperatures at which the isotope is likely to be used. This work is performed by the processing codes [3-9] using different approximations to get the values of $\sigma_x^l(E_m,\sigma_0)$ at different temperatures. Hence, a set of cross sections as a function of σ_0 and *T* is made available to transport codes for taking into account the effect of self-shielding.

The interpolation of the self-shielded cross sections on the σ_0 grid is the method applied by most of the deterministic transport codes. The probability table method [3,7,10] is more suitable for Monte Carlo simulations. The multiband method [1, 2] has been successfully applied both to deterministic and Monte Carlo codes.

2. Processing La-139 in the unresolved resonance region from FENDL using NJOY2016.60

The La-139 evaluation for FENDL-3.1c contains unresolved resonance data between 35.6157 keV and 164.1994 keV. The average level spacing, competing reaction widths, reduced neutron widths and radiation widths are given at 12 energy points.

The NJOY2016.60 nuclear data processing system was applied to prepare ACE-formatted files for Monte Carlo simulations and the MATXS-formatted file for deterministic calculations. The treatment of the self-shielding in the unresolved resonance range was performed using the PURR module. PURR samples ladders of resonances from the unresolved resonance parameters and computes probability tables (PTABLE) for Monte Carlo codes and Bondarenko cross sections as a function of the lumped cross section σ_0 for multigroup calculations. The σ_0 parameter takes into account the self-shielding effect. The value of $\sigma_0=\infty$ gives the unshielded cross section and $\sigma_0=0$ defines the fully shielded cross section.

In the case of La-139, PURR adds another 4 points using parameter interpolation to make a denser energy grid in the unresolved resonance region (URR). Then, it computes probability tables and Bondarenko cross sections at 12+4=16 energy points.

Users reported problems with FENDL processed data when they were analyzing a numerical benchmark for La-139 [11]. The geometry of the benchmark consisted in a 100 cm radius sphere of La-139 surrounded by a layer of 60 cm of air. An isotropic neutron source was located at the center emitting particles with an energy close to 20 MeV (19.64-20.00 MeV). In the original work by Konno [11], the energy of the source was set between 17.33 and 19.64 MeV.

Figure 1 shows that the averaged total neutron flux calculated using MATXS-formatted file and the ANISN [12] code is significantly different, and lower by up to 50% in the URR, to the one obtained applying MCNP6 [10] and the ACE-formatted file in the URR at the spatial interval (59.5 cm, 60.0 cm). The symbols MCNP-LA and ANISN-LA indicate that the corresponding ACE- and MATXS-formatted files were processed using NJOY2016.60 from Los Alamos National Laboratory (LANL).

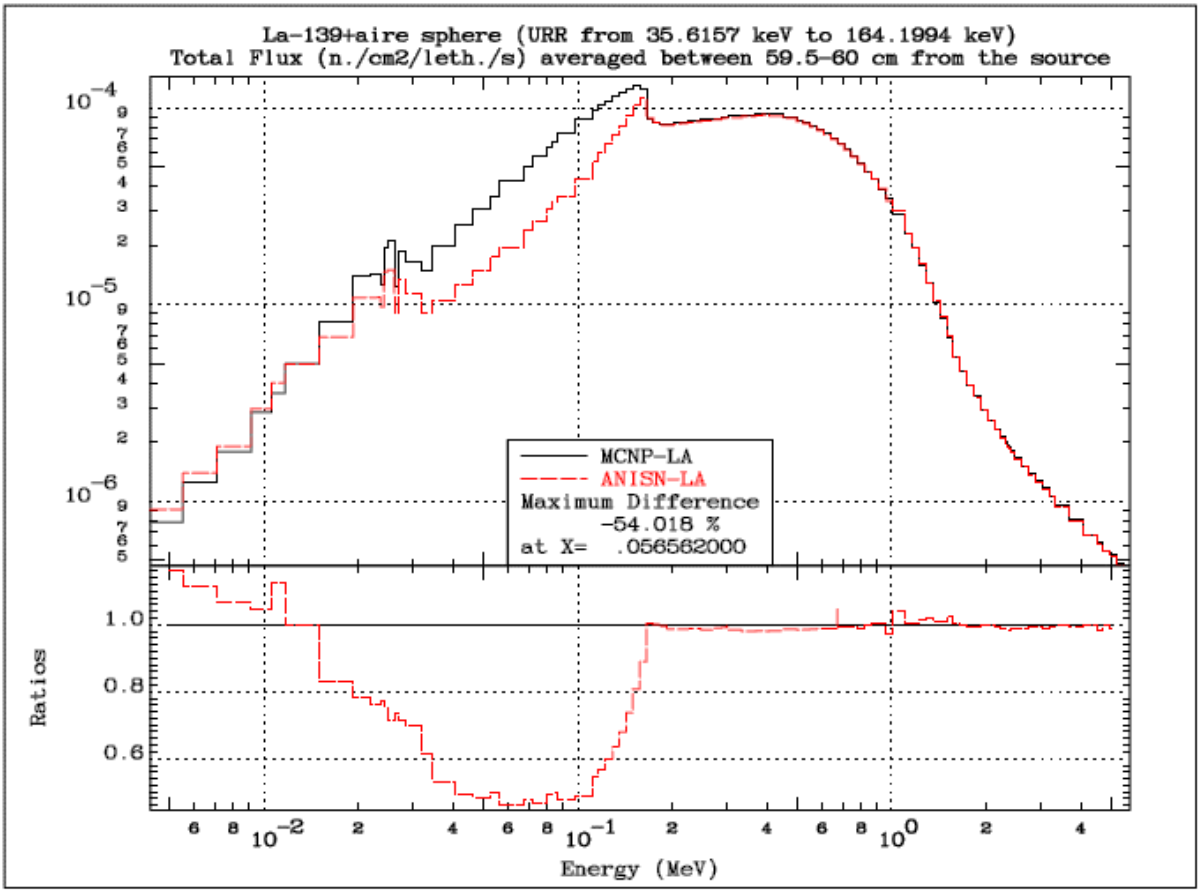

FIG. 1. Averaged total neutron flux at 60 cm distance from the source using NJOY2016.60 from Los Alamos National Laboratory (LANL)

Similarly, Fig. 2 presents the results for the total current at the external surface. Here, the differences are between -30% and +60% in the unresolved resonance region. It seems from the figures that the evaluated cross section may have a discontinuity at both the lower and higher boundaries of the URR.

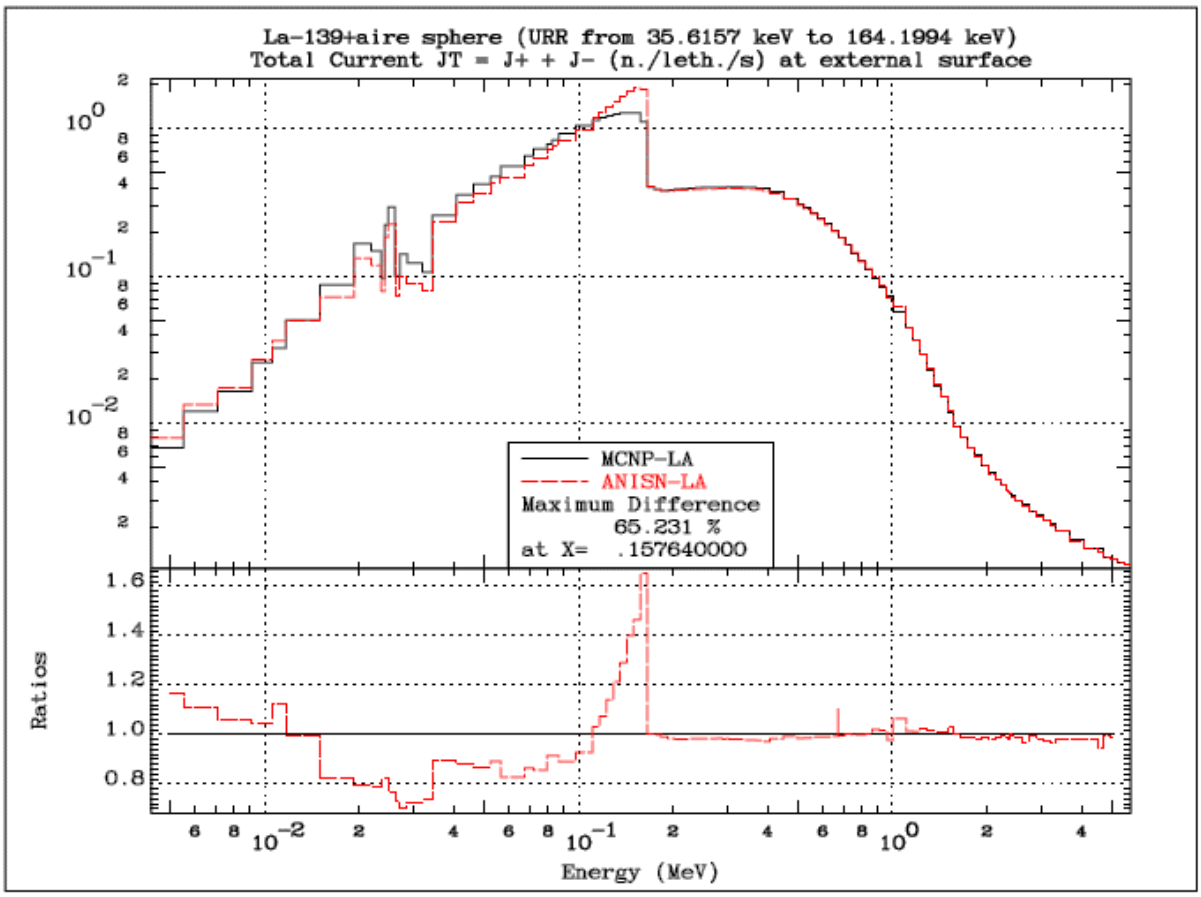

FIG. 2. Total neutron current at external surface using NJOY2016.60 from Los Alamos National Laboratory (LANL)

In the case of analyzed benchmark, the value of σ_0 is around 0.28 barn for La-139, if the constant escape cross section model is applied for self-shielding in the Bondarenko approach. The values of $\sigma_0 = 0.3$ barn and $\sigma_0 = 0.1$ barn were defined during the nuclear data processing. The code TRANSX [13] was applied for preparing the multigroup cross section data required by ANISN. The shielded cross sections at 0.28 barn were computed by interpolation on the σ_0 grid.

Recently, Konno suggested a patch [11] for solving the above-mentioned issue in the processed multigroup cross sections (MATXS). The patch in practice limits the higher boundary of the lower probability bin (σ_{tmax}^{bin1}) to the tenth part of the unshielded total cross section for each temperature at each energy point at which unresolved resonance data are given:

$$\sigma_{tmax}^{bin1} = \sigma_t(\sigma_0 = \infty)/10 \quad (5)$$

Konno's patch is similar to the approach used by the NJOY99 until version 99.83. At that point, a similar limiting condition was applied, but the potential cross-section (σ_{pot}) was used instead of the unshielded total cross section. Here, the allowed minimum total cross section value for computing the higher energy boundary of the first probability bin is set to $\sigma_{pot}/10$. The limiting condition defined from the potential

scattering cross section is a better choice from the physical point of view than the unshielded total cross section.

In the NJOY99.84 the sampling scheme was modified to use a different set of total cross section bins for each temperature. The binning logic was also changed to use approximately equally probable bins over most of the range with two bins of lower probabilities at the low and high ends. Furthermore, the limiting condition of $\sigma_{pot}/10$ was abandoned.

Later, in version NJOY99.296, the binning logic for the total cross section was changed again to provide more low probability intervals at the low and high wings. A value of (nbin-10) roughly equal probability bins were used in the central region and 5 lower probability bins are reserved for each wing, using declining probabilities going down or up in cross section. This patch also increased the number of samples and set for section MT152 the Bondarenko cross sections renormalized to the value calculated by direct sampling instead of the renormalized values computed from the probability table. In this way, the Bondarenko cross sections are independent of the binning procedure, but it represents a risk to the consistency between Monte Carlo and deterministic calculations. This patch represents the way that the binning and sampling procedures are implemented on the current version of NJOY2016 from LANL.

Limiting the first bin boundaries was not enough in the case of La-139, for which very small values of σ_0 are required. The idea to limit the total cross section comes from the fact that the single level Breit-Wigner formalism can produce unreasonable small values for the cross sections between resonances due to the neglect of interference and multi-channel effects. Therefore, PURR methods for small σ_0 values may render unrealistic results, because the term $[\sigma_t(E)+\sigma_0]$ in Eqs. (3) and (4) becomes very small (tends to zero). The problem is worse for the first order moment of the total cross section for which the weighting function is inversely proportional to $[\sigma_t(E)+\sigma_0]^2$.

A general overview of the problem would be addressed based on the work presented in references [1, 2] for the multiband method. Let's rewrite Eq. (3) as:

$$\sigma_x(E_m,\sigma_0)=\frac{\int_{E_1}^{E_2}\int_{\sigma_t min}^{\sigma_t max}\left\{\frac{\sigma_x(E)\,C(E)}{[\sigma+\sigma_0]}\delta[\sigma-\sigma_t(E)]\right\}d\sigma dE}{\int_{E_1}^{E_2}\int_{\sigma_t min}^{\sigma_t max}\left\{\frac{C(E)}{[\sigma+\sigma_0]}\delta[\sigma-\sigma_t(E)]\right\}d\sigma dE} \tag{6}$$

Where σ is an integration variable in the range of the total cross section and the symbol δ is the Dirac δ function. Eq. (6) is reduced to Eq. (3) if the integration over the total cross section σ is computed first. Due to mathematical properties of the integrand, the integration order can be changed. Then, if the integration over energy is performed first, we can obtain the basic expressions used in PURR:

$$\sigma_x(E_m,\sigma_0)=\frac{\int_{\sigma_t min}^{\sigma_t max}\left\{\int_{E_1}^{E_2}\{\sigma_x(E)C(E)\delta[\sigma-\sigma_t(E)]\}dE\right\}\frac{1}{[\sigma+\sigma_0]}d\sigma}{\int_{\sigma_t min}^{\sigma_t max}\left\{\int_{E_1}^{E_2}\{C(E)\delta[\sigma-\sigma_t(E)]\}dE\right\}\frac{1}{[\sigma+\sigma_0]}d\sigma} \tag{7}$$

The PURR module assumes that $C(E) \approx C = cte.$ between energies E_1 and E_2, therefore

$$\sigma_x(E_m, \sigma_0) = \frac{\int_{\sigma_t min}^{\sigma_t max} \left\{\int_{E_1}^{E_2} \{\sigma_x(E)\delta[\sigma - \sigma_t(E)]\} dE\right\} \frac{1}{[\sigma + \sigma_0]} d\sigma}{\int_{\sigma_t min}^{\sigma_t max} \left\{\int_{E_1}^{E_2} \{\delta[\sigma - \sigma_t(E)]\} dE\right\} \frac{1}{[\sigma + \sigma_0]} d\sigma} \quad (8)$$

Defining $P(\sigma)$ and $\sigma_x(\sigma)$ as:

$$P(\sigma) = \int_{E_1}^{E_2} \{\delta[\sigma - \sigma_t(E)]\} dE \quad (9)$$

$$\sigma_x(\sigma) P(\sigma) = \int_{E_1}^{E_2} \{\sigma_x(E)\delta[\sigma - \sigma_t(E)]\} dE \quad (10)$$

Equation (8) can be written as:

$$\sigma_x(E_m, \sigma_0) = \frac{\int_{\sigma_t min}^{\sigma_t max} \left\{\sigma_x(\sigma) \frac{1}{[\sigma + \sigma_0]} P(\sigma)\right\} d\sigma}{\int_{\sigma_t min}^{\sigma_t max} \left\{\frac{1}{[\sigma + \sigma_0]} P(\sigma)\right\} d\sigma} \quad (11)$$

The parameter $P(\sigma)$ can be interpreted as the total cross section probability density function and $\sigma_x(\sigma)$ represents the value of the cross section for reaction x as a function of the total cross section.

The PURR module builds an energy grid of 10000 (*nsamp*) values sampling uniformly energies between E_1 and E_2. Then, according to the evaluated data in the unresolved resonance range, it samples pointwise resonance parameters for each resonance sequence and accumulates the contributions to the cross sections in each equiprobable energy E_i. The values of $\sigma_t(E_i)$ can be considered as the discrete probability density function for the resonant cross section in the unresolved resonance range. Mathematically, it is equivalent to define the probability density function of the total cross section $P(\sigma)$ as:

$$P(\sigma) = \sum_{i=1}^{nsamp} \frac{1}{nsamp} \delta[\sigma - \sigma_t(E_i)] \quad (12)$$

Therefore, Eq. (11) reduces:

$$\sigma_x(E_m, \sigma_0) = \frac{\sum_i \frac{\sigma_x(E_i)}{[\sigma_t(E_i) + \sigma_0]}}{\sum_i \frac{1}{[\sigma_t(E_i) + \sigma_0]}} \quad (13)$$

Moreover, following the same approach for $\sigma_t^1(E_m, \sigma_0)$, Eq. (4) can be written as

$$\sigma_t^1(E_m, \sigma_0) = \frac{\sum_i \frac{\sigma_t(E_i)}{[\sigma_t(E_i) + \sigma_0]^2}}{\sum_i \frac{1}{[\sigma_t(E_i) + \sigma_0]^2}} \quad (14)$$

For infinite dilution $\sigma_0 = \infty$, $\sigma_t(E_i) \ll \sigma_0$ and Eq. (13) is reduced to

$$\sigma_x(E_m, \sigma_0) = \frac{1}{nsamp}\sum_i \sigma_x(E_i) \tag{15}$$

If due to the evaluated nuclear data quality and method limitations, a large amount of very small total cross sections is sampled, then Eqs. (13) and (15) can produce wrong results.

If we have a set of *ntot* samples out of the total *nsamp* set of samples that fulfill the condition

$$\sigma_t(E_j) \ll \sigma_0, \quad j = 1, \ldots ntot < nsamp \tag{16}$$

Then, Eqs. (13) and (14) can be written as:

$$\sigma_x(E_m, \sigma_0) = \frac{\sum_{i=1}^{nsamp-ntot} \frac{\sigma_t(E_i)}{[\sigma_t(E_i)+\sigma_0]} + \frac{1}{\sigma_0}\sum_{j=1}^{ntot}\sigma_t(E_j)}{\sum_{i=1}^{nsamp-ntot} \frac{1}{[\sigma_t(E_i)+\sigma_0]} + \frac{1}{\sigma_0}ntot} \tag{17}$$

$$\sigma_t^1(E_m, \sigma_0) = \frac{\sum_{i=1}^{nsamp-ntot} \frac{\sigma_t(E_i)}{[\sigma_t(E_i)+\sigma_0]^2} + \frac{1}{\sigma_0^2}\sum_{j=1}^{ntot}\sigma_t(E_i)}{\sum_{i=1}^{nsamp-ntot} \frac{1}{[\sigma_t(E_i)+\sigma_0]^2} + \frac{1}{\sigma_0^2}ntot} \tag{18}$$

Due to the condition (16), the second term in the numerator of Eqs. (17) and (18) can be neglected, and the equations rewritten as

$$\sigma_x(E_m, \sigma_0) = \frac{\sum_{i=1}^{nsamp-ntot} \frac{\sigma_t(E_i)}{[\sigma_t(E_i)+\sigma_0]}}{\sum_{i=1}^{nsamp-ntot} \frac{1}{[\sigma_t(E_i)+\sigma_0]} + \frac{1}{\sigma_0}ntot} \tag{19}$$

$$\sigma_t^1(E_m, \sigma_0) = \frac{\sum_{i=1}^{nsamp-ntot} \frac{\sigma_t(E_i)}{[\sigma_t(E_i)+\sigma_0]^2}}{\sum_{i=1}^{nsamp-ntot} \frac{1}{[\sigma_t(E_i)+\sigma_0]^2} + \frac{1}{\sigma_0^2}ntot} \tag{20}$$

From these equations we can see that for small σ_0 ($\sigma_0 < 1\ barn$) and large *ntot* the terms $\frac{1}{\sigma_0}ntot$ and $\frac{1}{\sigma_0^2}ntot$ become too large, therefore the value of the calculated Bondarenko cross sections is underestimated.

One of the worst-case scenarios is realized for the evaluated La-139 cross section, where you can find very small $\sigma_t(E_i)$ values for more than 225 samples, then for $\sigma_0 = 0.1\ barn$ the term $\frac{1}{\sigma_0}ntot$ is greater than 2250 and the term $\frac{1}{\sigma_0^2}ntot$ is greater than 22500. Those terms represent more than 22.5% and the 225% of the total number of samples, respectively for the zero and first moment. In a similar way the

probability tables are affected, even if some dependency on the binning strategy is observed for the probability tables.

If $\sigma_0 \gg ntot$, then the second term in the denominator of Eqs (19) and (20) can also be neglected and the problem is diminished. In this case $\sigma_x(E_m,\sigma_0)$ and $\sigma_t^1(E_m,\sigma_0)$ can be computed as:

$$\sigma_x(E_m,\sigma_0) = \frac{\sum_{i=1}^{nsamp-ntot} \frac{\sigma_t(E_i)}{[\sigma_t(E_i)+\sigma_0]}}{\sum_{i=1}^{nsamp-ntot} \frac{1}{[\sigma_t(E_i)+\sigma_0]}} \quad (21)$$

$$\sigma_t^1(E_m,\sigma_0) = \frac{\sum_{i=1}^{nsamp-ntot} \frac{\sigma_t(E_i)}{[\sigma_t(E_i)+\sigma_0]^2}}{\sum_{i=1}^{nsamp-ntot} \frac{1}{[\sigma_t(E_i)+\sigma_0]^2}} \quad (22)$$

A patch for PURR was prepared to address this issue based on the above arguments. The patch rejects the set of samples with a total cross section value below $\sigma_{pot}/10$. The way to select the bins boundaries was consistently modified. The values of Bondarenko cross sections that are saved on section MF2/MT152 are those computed from the probability tables after renormalization to the unshielded cross section calculated from averaged unresolved resonance data on section MF2/MT151. These Bondarenko cross sections are consistent with the probability tables saved on section MF2/MT153.

It might be possible to customize the change of the minimum total cross section to a value of $f \cdot \sigma_{pot}$, where the factor f is a predefined (input) fraction ($0< f \leq 1/10$). The value of zero means no limitation and the factor of 1/10 is the value in the current patch. It could be introduced as an input parameter for PURR calculations; this is a suggestion for NJOY developers.

Figures 3 and 4 show the results obtained applying this patch taking the minimal total cross section equal to $\sigma_{pot}/10$. The maximum differences between MCNP and ANISN calculations for the total neutron flux are now 20% in the URR, which means an improvement of 30% comparing with the case of no patching applied. Concerning the total neutron current at the external surface shown in Fig. 4, the differences lie in the interval between -10% and +10%, which also represents a significant reduction of the differences.

To have a better picture of the impact of the patch, Figs 5 and 6 summarize the results of La-139 processing from FENDL using NJOY2016.60 without and with patching. It is worthy to note that the patch affects both deterministic (50% increase in the neutron flux) and Monte Carlo (30% increase in the neutron flux) calculations, because it does change the Bondarenko cross sections, but also the probability tables.

The agreement in the calculated current between the deterministic and the MC calculations is excellent after the patch is applied as shown in Fig. 6. The processing of main actinides in FENDL-3.1c library were insensitive to the patch.

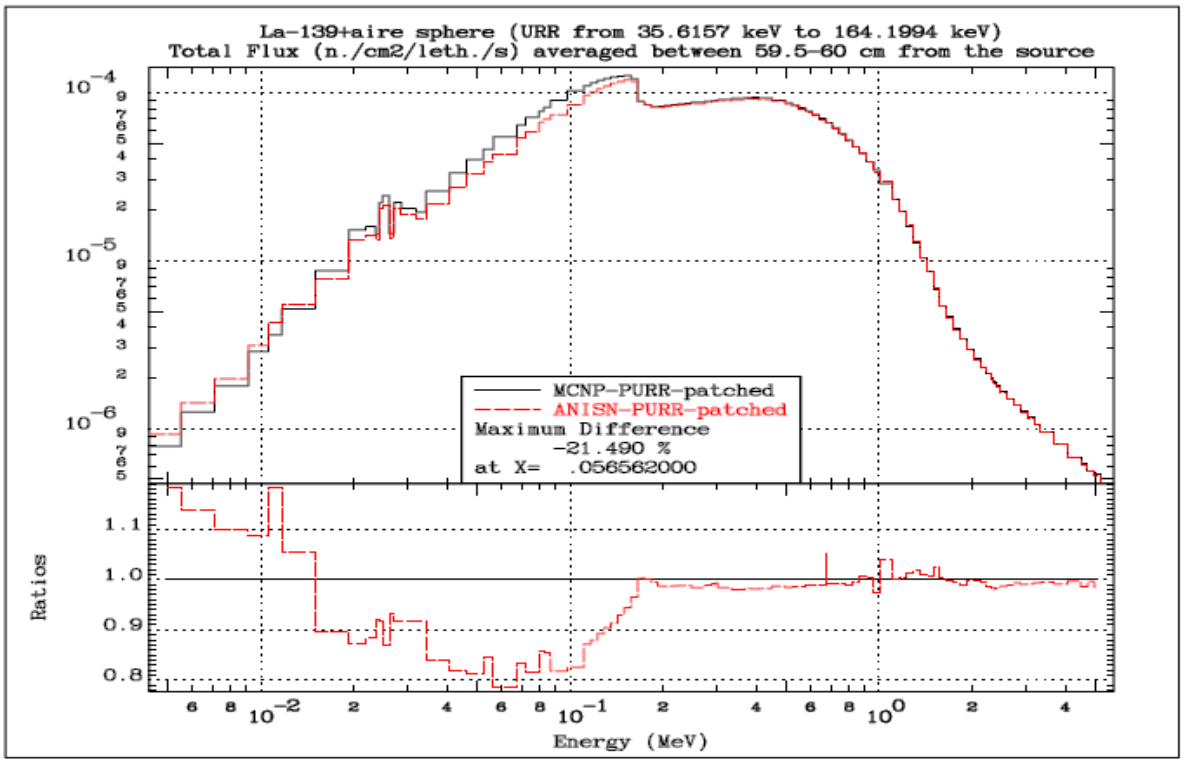

FIG. 3. Averaged total neutron flux at 60 cm distance from the source using NJOY2016.60 with PURR patched ($\sigma_t^{min}(E) = \sigma_{pot}/10$).

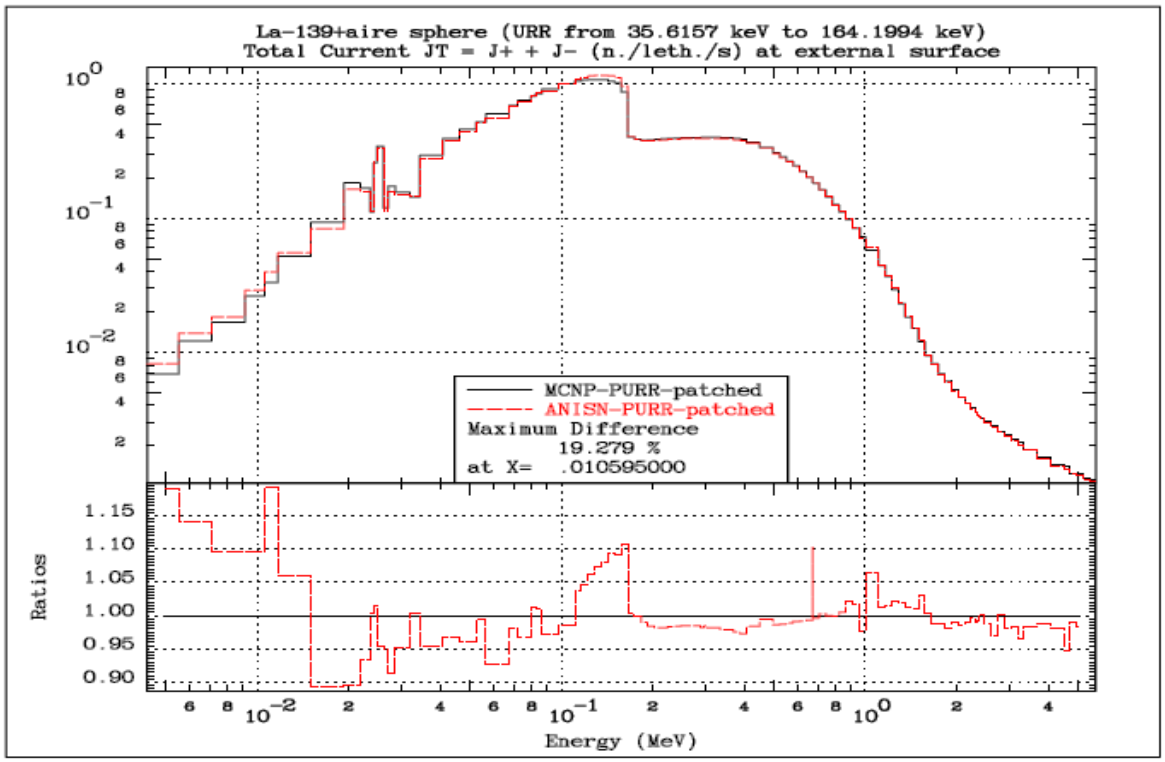

FIG. 4. Total neutron current at external surface using NJOY2016.60 with PURR patched ($\sigma_t^{min}(E) = \sigma_{pot}/10$)

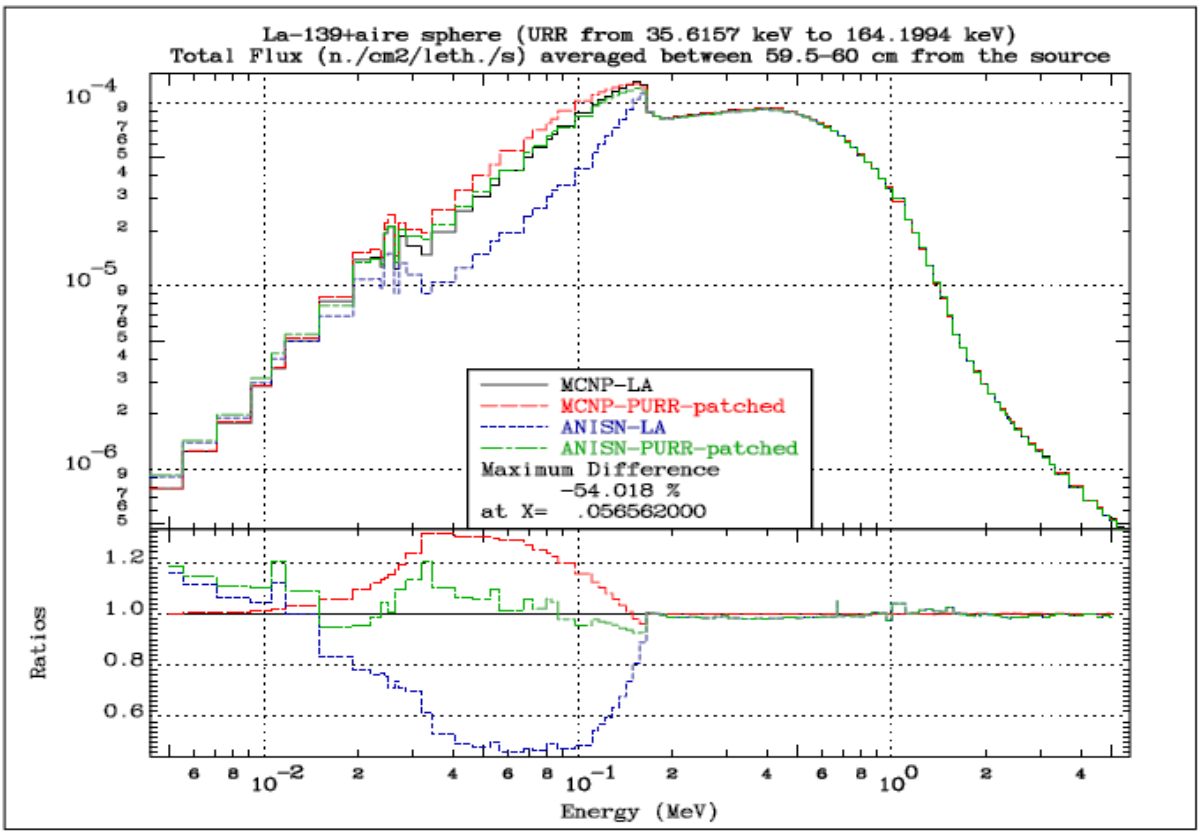

FIG. 5. Comparison of averaged total neutron flux at 60 cm distance from the source using NJOY2016.60 without and with PURR patched ($\sigma_t^{min}(E) = \sigma_{pot}/10$)

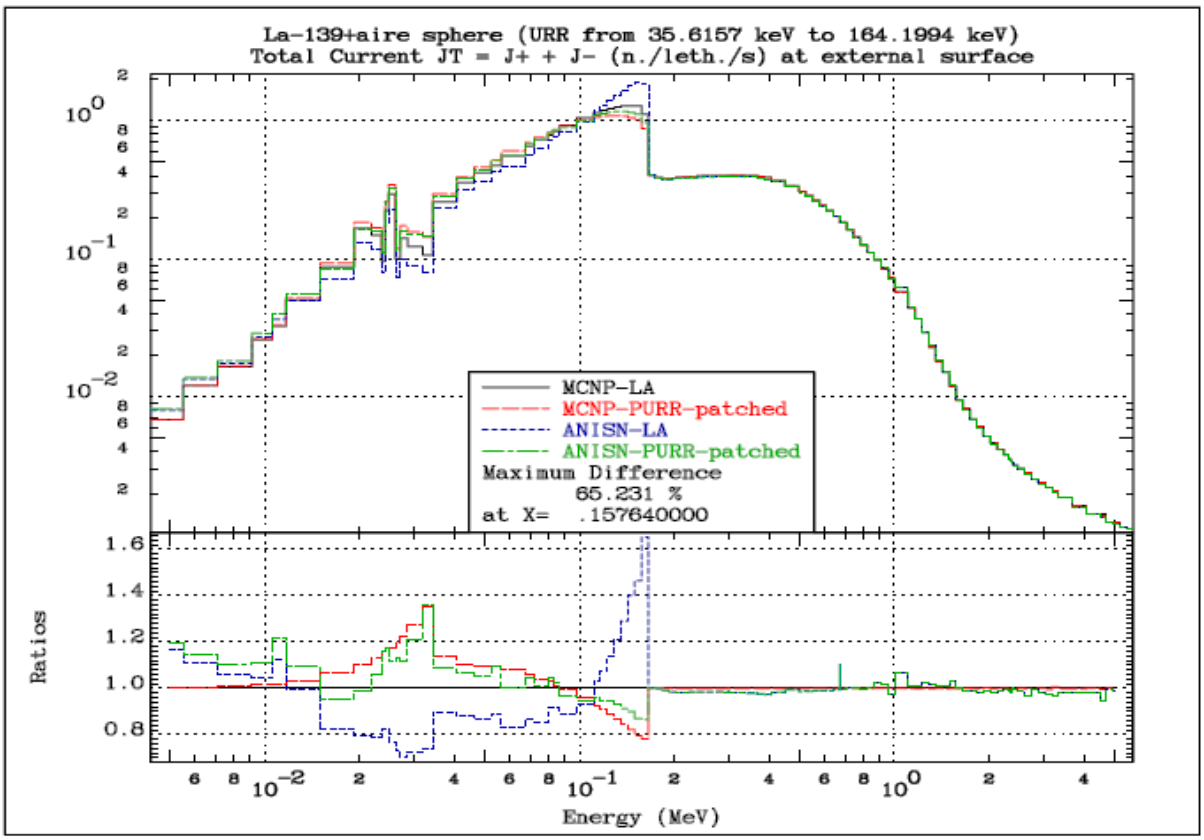

FIG. 6. Comparison of total neutron current at external surface using NJOY2016.60 without and with PURR patched ($\sigma_t^{min}(E) = \sigma_{pot}/10$)

Additionally, Figs 7 and 8 show the results obtained using NJOY2016.60 with and without the patch but using evaluated data from ENDF/B-VIII.0 for La-139. Comparing Figs 4 and 5 with 8 and 9 respectively, it can be seen a similar behavior. However, the impact of the patch is reduced; Monte Carlo calculations with the patched NJOY differ less than 5% from the original, whilst the deterministic calculation is improved by about 20% in the unresolved resonance region.

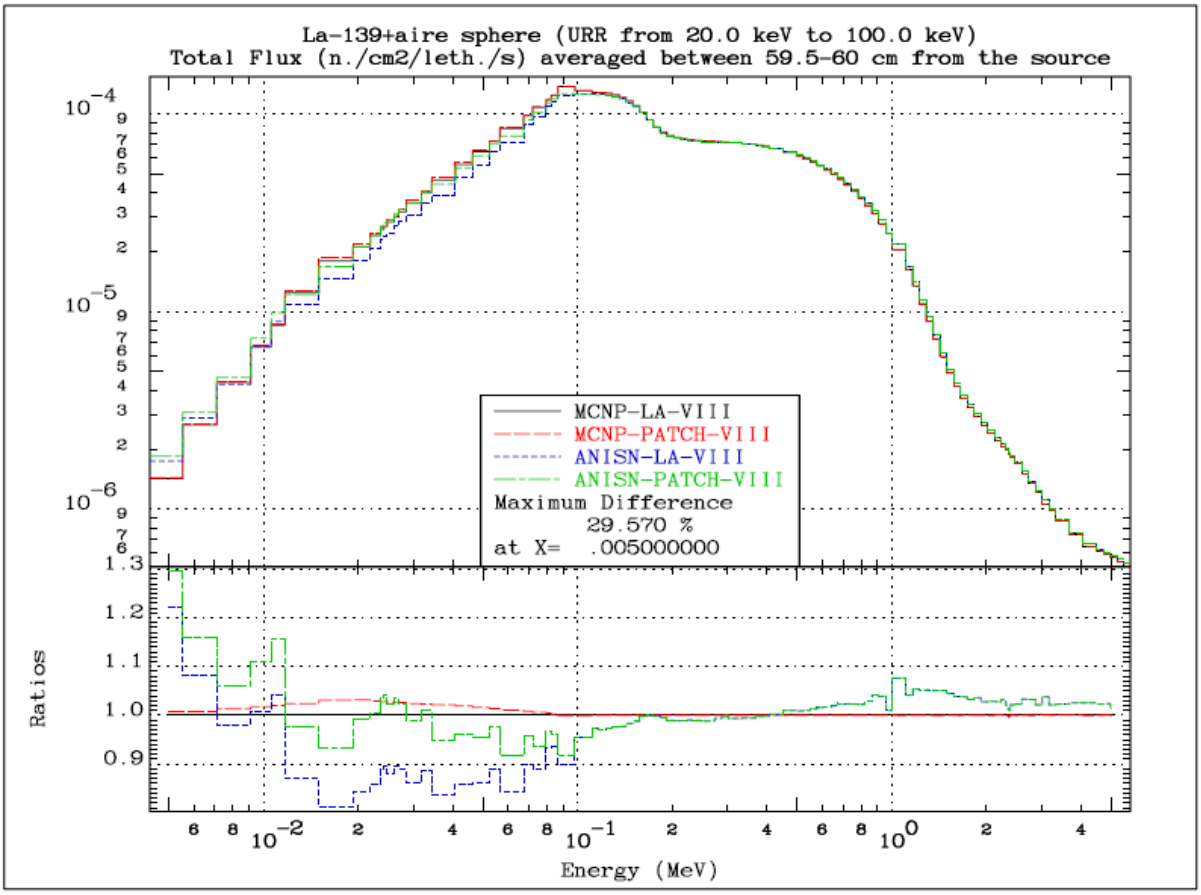

FIG. 7. Comparison of averaged total neutron flux at 60 cm distance from the source using NJOY2016.60 without and with PURR patched for La-139 from ENDF/B-VIII.0

While the resulting differences are reduced compared to the FENDL evaluation, this is not related to processing issues, but to issues in the evaluated data in the URR, especially in the FENDL evaluation. Issues related with La-139 evaluation in the unresolved resonance range have been reported in Ref. [14].

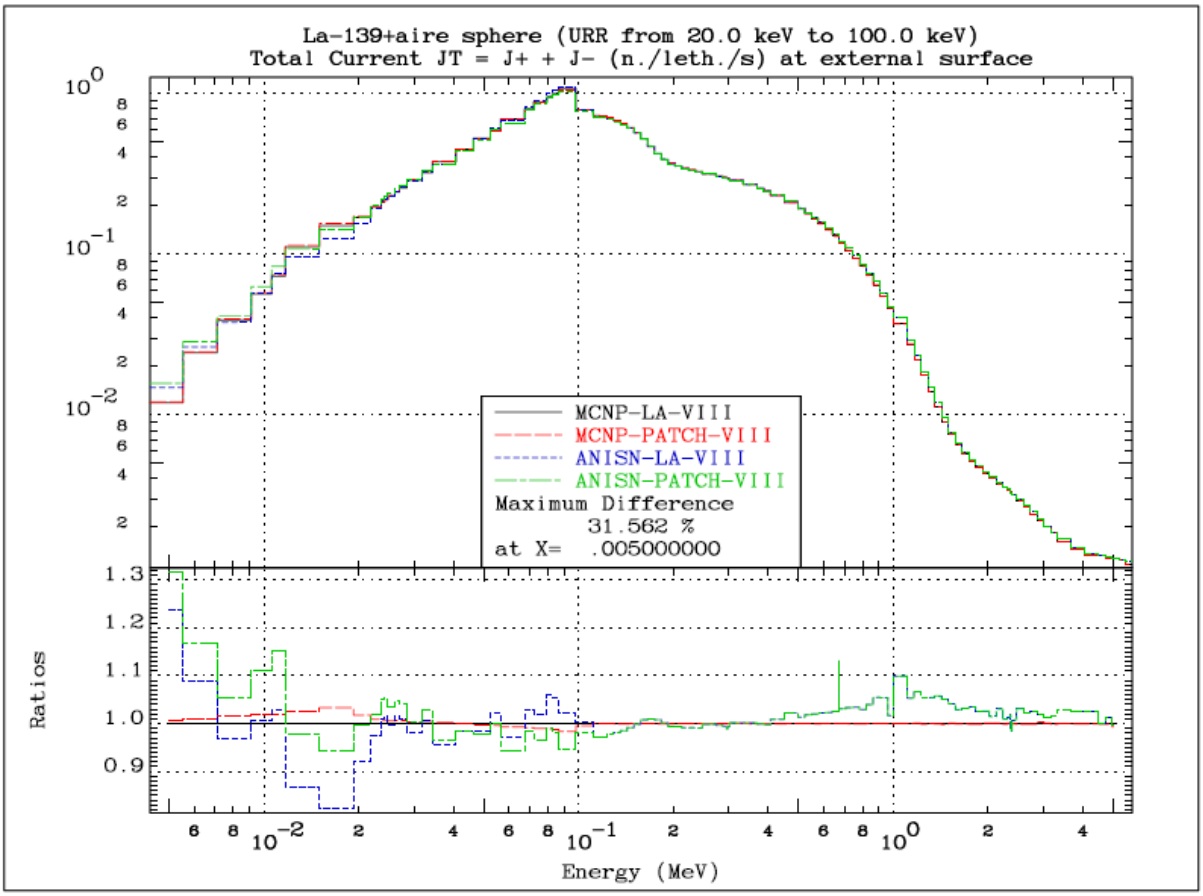

FIG. 8. Comparison of total current at external surface using NJOY2016.60 without and with PURR patched for La-139 from ENDF/B-VIII.0

3. Final remarks

A patch for NJOY2016/PURR has been proposed to correct a problem in self-shielding calculations in the URR when a large number of samples with very small values of the total cross section are generated in PURR. The patch essence is the rejection of the samples with a value of total cross section smaller than $\sigma_{pot}/10$. Warning messages are printed. This patch achieves a better consistency between Monte Carlo and deterministic calculations of the analyzed numerical benchmark suggested by Konno for a 20 MeV neutron source at the center of 1-meter sphere of La-139.

This patch has been verified to be insensitive for the processing of main actinides for the FENDL-3.1c library. Further tests are warranted.

Konno's benchmark is very sensitive to the quality of the URR processing as well as to the quality of evaluated data in that region and may be recommended for a QA of the URR evaluations. The patch increases the neutron flux in the URR for Monte Carlo calculations (4% increase for the ENDF/B-VIII.0 evaluation vs 30% for the FENDL-3.1c evaluation). The corresponding increase of the calculated neutron flux for deterministic codes goes from 15% for the ENDF/B-VIII.0 data up to 50% for the FENDL-3.1c, accordingly. Such non-negligible differences for deterministic calculations make a strong case for the modification of the current NJOY code.

The comparison of the results obtained by using the probability tables and Bondarenko cross section from NJOY/PURR module and by applying the methods of GROUPIE/URRFIT codes as well as the analysis of Konno's benchmark using ENDF/B-VIII.0 data suggests a revision of the evaluated unresolved resonance data of La-139 to achieve consistency between the resonance, the URR and the fast neutron region [14].

It is recommended to continue exploring this issue to improve processing methods and evaluated data quality.

References

[1] Cullen D.E., Nuclear Cross Section Preparation" In Ronen Y. (Ed), Handbook of Nuclear Reactor Calculations, Volume I, CRC Press, Boca Raton, FL (1986) 13-131.

[2] Cacuci, D.G. (Ed.), Handbook of Nuclear Engineering. Volume I, Nuclear Engineering Fundamentals, Springer, 2010.

[3] Kahler, A.C. (Ed.), The NJOY Nuclear Data Processing System, Version 2016, Report LA-UR-17-20093, Los Alamos National Laboratory, December 19, 2016.

[4] Sinitsa, V.V. (Ed.), GRUCON – a Package of Applied Computer Programs for Evaluated Nuclear Data Processing, User´s Manual, NRC Kurchatov Institute, December 2016.

[5] Cullen, D.E., Trkov, A., URR-PACK: Calculating Self-Shielding in the Unresolved Resonance Energy Range, Report INDC(NDC)-0711 Rev. 1, Nuclear Data Section, IAEA, Vienna, Austria, July 2016.

[6] Cullen, D.E., PREPRO 2018 2019 ENDF/B Pre-processing codes, Report IAEA-NDS-39 Rev.20, Nuclear Data Section, IAEA, Vienna, Austria, 2019.

[7] NEA-1278 CALENDF-2010, Pointwise, Multigroup neutron cross sections and probability tables from ENDF/B evaluations, NEA-DATA BANK, OECD, 2010.

[8] Kenichi, T., Nagaya, Y., Kunieda, S., Suyama, K., Fukahori, T., Development and verification of a new nuclear data processing system FRENDY, J. Nucl. Sci. Technol. **54**/7 (2017) 806.

[9] López Aldama, D., Cullen, D.E., Trkov, A., ACEMAKER-2019. A code package to produce ACE-formatted files for MCNP calculations, Report IAEA-NDS-223 Rev1, Nuclear Data Section, IAEA, Vienna, Austria, 2019.

[10] MCNP – A General Monte Carlo N-Particle Transport Code, Version 5, Volume I: Overview and Theory, X-5 Monte Carlo Team, Report LA-UR-03-1987, Los Alamos National Laboratory, April 24, 2003, (Revised 02/01/2008).

[11] Konno, C., Tada K., Kwon, S., MATXS multigroup file problem due to NJOY unresolved resonance processing, submitted to ICRS14/RPSD2020, 2020.

[12] Engle, W.W., A USER'S MANUAL FOR ANISN. A One Dimensional Discrete Ordinates Transport Code With Anisotropic Scattering, K-1693, Nuclear Division, Union Carbide Corporation, 1967.

[13] Macfarlane, R.E., TRANSX 2: a code for interfacing MATXS cross-section libraries to nuclear transport codes, Report LA-12312-MS, Los Alamos National Laboratory (1993).

[14] Trkov, A., Cullen, D.E., Lopez Aldama D., On the Self-Shielding in the Unresolved Resonance Range, Proceedings of the International Conference Nuclear Energy for New Europe, Portorož, Slovenia, September 7-10, 2020.

Nuclear Data Section
International Atomic Energy Agency
Vienna International Centre, P.O. Box 100
A-1400 Vienna, Austria

E-mail: nds.contact-point@iaea.org
Fax: (43-1) 26007
Telephone: (43-1) 2600 21725
Web: http://nds.iaea.org